A Film-Flow Model to Describe Free Water Transport during Drying of a Hygroscopic Capillary Porous Medium

Martine Goyeneche, Didier Lasseux, Denis Bruneau

Transport in Porous Media, *2002*, **48:** 125–158, DOI: 10.1023/A:1015646307537

A Film-Flow Model to Describe Free Water Transport during Drying of a Hygroscopic Capillary Porous Medium

MARTINE GOYENECHE, DIDIER LASSEUX and DENIS BRUNEAU
L.E.P.T.-ENSAM (UMR CNRS 8508), Esplanade des Arts et Métiers, 33405 Talence Cedex, France.

Abstract. In this work, a two-phase film-flow model in a hygroscopic capillary tube is developed and extended to describe the two-phase capillary viscous transport in a network of parallel capillary tubes in terms of relative permeabilities. This film-flow approach is further considered to predict the longitudinal moisture transport in oak wood during drying. Numerical results obtained from this prediction are compared with data of convective drying experiments performed on samples of this wood. The comparison seems to confirm the physical relevance of a film-flow model to correctly represent the moisture transfer until the hygroscopic regime is reached.

Key words: capillary porous medium, films, drying, irreducible saturation, relative permeabilities.

Nomenclature

a_w	water activity [-].
$A_{\kappa\xi}$	κ-ξ interface [m^2].
$B(\phi)$	resistance factor in the effective diffusitivity of vapor in the medium [-].
C	vapor mass fraction in the gas phase [-].
C_p	constant pressure heat capacity [J kg^{-1} K^{-1}].
D	diffusivity [m^2 s^{-1}].
e	film thickness [m].
$\mathbf{e_x}$	axial vector [-].
$\mathbf{e_r}$	radial vector [-].
F_m	mass flux [kg m^{-2} s^{-1}].
h	intrinsic averaged enthalpy [J kg^{-1}].
h_m	mass exchange coefficient [m s^{-1}].
h_T	heat exchange coefficient [W m^{-2} K^{-1}].
H	double mean curvature [m^{-1}].
$\overline{H}$	thermal mass [J m^{-3}].
$\mathbf{I}$	unit tensor [-].
K	intrinsic permeability [m^2].
$K_{r\kappa}$	κ-phase relative permeability [-].
$K_{r\kappa\xi}$	κ-phase/ξ-phase coupling relative permeability [-].
L_0	characteristic length of a capillary tube [m].

M_a	molar mass of air [kg mol^{-1}].
$\mathbf{n}_{\beta\alpha}$	unit normal vector to the $A_{\beta\alpha}$ interface directed from the β-phase towards the α-phase [-].
p_κ	κ-phase pressure [Pa].
Q	total heat flux [W m^{-2}].
R	gas constant [J K^{-1} mol^{-1}].
R_{max}	maximum pore radius [m].
R_{min}	minimum pore radius [m].
R_0	mean capillary radius [m].
S	free water saturation [-].
S_{irr}	irreducible saturation [-].
S_0	small saturation value close to 0 [-].
t	time [s].
T	temperature [K or °C].
$\mathbf{t}_{\alpha\beta}$	direct unit normal vector to $n_{\beta\alpha}$, tangential to the $A_{\beta\alpha}$ interface [-].
u_κ, v_κ	κ-phase axial and radial velocities in the capillary tube [m s^{-1}].
$\overline{u}_\kappa$, $\overline{v}_\kappa$	κ-phase axial and radial filtration velocity [m s^{-1}].
$\mathbf{V}_\kappa$	κ-phase local velocity [m s^{-1}].
$\overline{\mathbf{V}}_k$	κ-phase filtration velocity [m s^{-1}].
W	dry-based moisture content [-].
W_{sp}	dry-based bound water content at the saturation point [-].
x, r	space variables [m].

Greek symbols

α	gas-phase.
β	liquid-phase (free water).
ε	asymptotic development parameter [-].
ε_κ	volume fraction of the κ-phase [-].
ϕ	porosity, measured on a dry sample [-].
γ	interfacial tension between the α- and β-phase [N m^{-1}].
λ	effective thermal conductivity [W m^{-1} K^{-1}].
μ_κ	κ-phase dynamic viscosity [kg m^{-1} s^{-1}].
ρ_κ	κ-phase intrinsic density [kg m^{-3}].
σ	solid-phase.
$\mathbf{\Sigma}_\kappa$	stress tensor associated to the κ-phase [-].
$\Psi(r)$	pore radius distribution function [m].

Subscripts

a	dry air.
amb	ambient conditions.
b	bound water.
c	capillary.
ini	initial.
v	vapor.
v sat	saturate vapor.
α	gas (humid air).
β	liquid (free water).
σ	solid.

Superscripts

eff	effective.
α	gas.
β	liquid.

Mathematical operators

$\sim$	dimensionless variable.
$^-$	averaged value.
∇	gradient operator.
$\nabla.$	divergence operator.

1. Introduction

Physical phenomena involved during drying of hygroscopic capillary porous media have been often discussed for the last 20 years. By hygroscopic, it is meant that solvent (here water) is able to be adsorbed or desorbed on the solid skeleton depending on the thermodynamic conditions of the ambient humid air. In most of the studies, physical models used to describe moisture transfer at a given point of the porous material are based on the existence of two different stages referred to as *non-hygroscopic* and *hygroscopic*. During these two stages, drying corresponds to the transfer of *free* water and water *bound* to the solid matrix respectively (Perré and Degiovanni, 1990; Nadeau and Puiggali, 1995). By extension, the portion of the medium still occupied by free water is usually called the *non-hygroscopic region*, whereas the rest is the *hygroscopic region*. Free water refers to water retained in the larger pores by capillary forces while bound water refers to physically adsorbed water under multimolecular layers on the walls of the solid structure by Van der Waals and electrostatic forces. These short and long range forces play an important role since it is commonly accepted that for pores of less than 1 μm in radius, capillary flow cannot take place (Moyne, 1987; Couture, 1995).

To follow the evolution of the water content in the medium, one usually uses two different parameters: the *dry-based moisture content*, W, and the water saturation, S. While W is defined as the ratio between the mass of water and the mass of dry product, S represents the ratio between the free water volume and the pore volume:

$$S = \varepsilon_l / \phi. \tag{1}$$

In the non-hygroscopic region, S locally varies from 1 to 0 whereas bound water content remains to its maximum value, W_{sp}, corresponding to the so-called *saturation point* of the solid matrix. When local saturation falls to zero, the corresponding portion of the medium enters the hygroscopic region and bound water elimination starts. In this region, moisture removal actually results from a diffusion-sorption phenomenon and is often modeled by a diffusive process supplied by a gradient of bound water content.

During the overall drying process, Darcy's law is used to describe gas-phase momentum transport owing to the action of capillary pressure gradient, while simultaneously, a diffusion model is generally employed to describe vapor and dry air relative transfer within this phase using, for instance, Fick's law, or more accurately, a dusty gas model approach (Mason and Malinauskas, 1983).

In the present work, attention is focussed on the description of physical mechanisms involved in the non-hygroscopic region. A review of the literature indicates that this region is often divided into two sub-regions respectively called *'funicular'* and *'pendular'* separated by the *irreducible saturation point* at which $S = S_{irr}$ (Spolek and Plumb, 1981; Whitaker and Chou, 1983–1984; Kaviany and Mittal, 1987; Perré and Moyne, 1991; Puiggali and Quintard, 1992). Some work performed on a pure geometrical and mechanistic model applied to softwood (Comstock, 1970) and on capillary pressure measurement (Spolek and Plumb, 1981) seemed to justify the existence of such a point above which free water would remain continuous and below which free water would be discontinuous. On this basis, it was assumed that no liquid flow could occur in the pendular zone – $0 \leqslant S \leqslant S_{irr}$ – whereas, in the funicular zone – $S_{irr} \leqslant S \leqslant 1$ – moisture transfer was due to a continuous supply of liquid water towards the surfaces of the medium. In this later zone, the use of the generalized Darcy's law is always admitted. Assuming the existence of an irreducible saturation point, it was successfully applied, for instance, to study drying in the funicular region of a non-hygroscopic medium made of glass beads from an experimental and analytical point of view (Kaviany and Mittal, 1987). However, strong arguments were raised to show that convective transport of humid air combined with diffusive vapor transfer in this gas phase within the porous medium was absolutely not sufficient to explain the rate of water extraction in the pendular zone (Whitaker and Chou, 1983–1984). This was confirmed by others (Moyne, 1987) in agreement with an experimental work (Ceaglske and Hougen, 1937). To circumvent this difficulty, Whitaker and Chou suggested to replace the pendular zone by an artificial saturation jump from $S = S_{irr}$ to $S = 0$ in a formal manner. Their comparison with experimental data obtained from convective drying on granular porous media showed a poor agreement for $S < S_{irr}$ leading to the conclusion that this approach was not satisfactory.

From this conclusion, an alternative idea was put forth to accept that some liquid-phase mass transport must occur down to a saturation S_0 less than S_{irr} and very close to 0 (Whitaker, 1984). By artificially adjusting the capillary pressure and liquid phase relative permeability between S_{irr} and S_0, Whitaker showed that a good agreement between theory and experiment could be achieved. Nevertheless, it was not clear how one could physically justify the way these parameters must be modified, the only argument was that S_0 can not be distinguished from zero while capillary pressure and relative permeability can not be determined experimentally in this rang of saturation. Since then, this latter approach has been followed by most of authors (Perré and Degiovanni, 1990; Perré and Moyne, 1991; Puiggali and Quintard, 1992; Ferguson and Turner, 1994; Couture *et al.*, 1996; Perré and Turner, 1999) with the thought that the liquid phase remains continuous below S_{irr} through connected wetting liquid films. If the medium is not totally non-hygroscopic, this seems reasonable to our opinion. In fact, few molecule layers adsorbed on the skeleton are sufficient to enhance the development of thick enough films in corners and surface roughness able to ensure capillary transfer of free water leading to a

slow but non-zero liquid flow. Those films are probably not thick enough for other effects like Van der Waals and electrostatic forces to be neglected in comparison to capillary effects. These long and short range forces are usually considered by using a disjoining pressure concept. In the preset work, no disjoining pressure is introduced in the development and for this reason, results derived here must be considered in the range of thick enough films.

More recently, drying experiments were performed under stationary and non-stationary conditions on two-dimensional transparent etched networks with an open end subjected to evaporation (Laurindo, 1996). Phase distributions were followed visually and well reproduced by a discrete numerical model based on a pure diffusive mass transfer (Laurindo and Prat, 1998a). However, predicted drying rates compared poorly with experimental data and this was attributed to the role of liquid films that were not taken into account in the numerical model (Laurindo and Prat, 1998b). Experimental evidence of the presence of these films in the network was clearly demonstrated by the same authors and was emphasized by additional observations on beds made of smooth and rough beads respectively, confirming some earlier work (Dullien *et al*., 1989). This provides an additional strong argument in favor of an extension of the funicular zone down to extremely low saturations.

Our aim in this work is to investigate the possibility of using a generalized Darcy's law to model the moisture transfer during drying of a capillary porous medium in the overall non-hygroscopic domain. For this purpose, keeping the idea that films maintain liquid transport, we use a two-phase film-flow model on a simplified structure of a porous medium in order to predict the relative permeability-saturation relationship *without any adjustment*. The simplified geometrical model used in this work is a bundle of capillary tubes while simplifying assumptions are made on the distribution of fluid phases within each tube. To begin with, the flow model is derived in the case of a single tube. It is further extended to the case of a bundle of tubes and the resulting relationship between relative permeability and saturation is employed in a computational drying model. Computational results are finally compared with data obtained from convective drying experiments performed on a sample of oak wood in the longitudinal direction. Comments are provided regarding values of the permeabilities resulting from the fluid distribution assumed in the present work.

2. Film-Flow Model

In this section, a two-phase film-flow model is proposed in order to describe free water transfer in a hygroscopic porous medium. To begin with, the two-phase Stokes problem is solved in a single capillary tube. A 1D solution is first obtained by making use of the classical lubrication approximation and is compared with a 2D one obtained from an asymptotic development.

Starting from this result, the film-flow model is extended to the case of a bundle of capillary tubes considered as a model of a capillary porous medium. To do

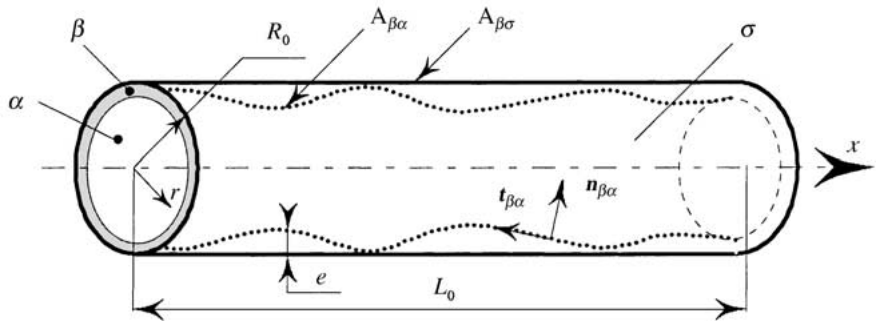

Figure 1. Cylindrical capillary tube.

so, free water is assumed to be distributed under the form of wetting films and gas phase to occupy the center of the pores, allowing the estimation of relative permeability-saturation relationships that are further used for numerical simulations of a drying process.

2.1. A FILM-FLOW MODEL IN A SINGLE CYLINDRICAL CAPILLARY TUBE

The system under consideration is depicted in Figure 1 where we have represented a portion L_0 of a cylindrical capillary tube – σ-phase – of circular cross section which inner radius is R_0. The inner wall is supposed to be covered by a wetting film – β-phase – of local thickness $e(x)$, while the non-wetting fluid – α-phase – flows in the center of the tube. A similar system of equations was considered for the solution of the film-thickness far from the meniscus during drainage of a capillary tube (Derjaguin, 1943; Lasseux and Quintard, 1991; Quéré, 1999). One is now interested in deriving a simplified solution of the two-phase flow in this configuration.

In what follows, L_0 is supposed to be infinitely large in comparison to R_0. In addition, we assume that the problem is axisymetric, stationary and that both phases are newtonian, incompressible and flow at a sufficiently low Reynolds number for the Stokes approximation to be valid. Gravity is neglected since this term will assume to have no contribution in the drying process. We neglect Van der Waals and electrostatic forces and we further make the hypothesis that no shear and phase-change occur on the β-α interface. Surface elasticity, surface viscosity and convective momentum transport are supposed to be negligible on this surface while the classical no slip condition applies on the β-σ interface. The associated boundary value problem may hence be stated as follows

• *α-phase (gas):*

– mass balance

$$\nabla.\mathbf{V}_\alpha = 0, \tag{2}$$

– momentum balance

$$0 = -\nabla p_\alpha + \mu_\alpha \nabla^2 \mathbf{V}_\alpha. \tag{3}$$

• *α-β interface ($r = R_0 - e(x)$):*

B.C. 1 $\quad \mathbf{V}_\alpha = \mathbf{V}_\beta \quad$ on $\; A_{\alpha\beta}$, (4)

B.C. 2 $\quad [\mathbf{n}_{\beta\alpha}.\Sigma] = \mathbf{n}_{\beta\alpha} \cdot (\Sigma_\beta - \Sigma_\alpha) = \gamma H \mathbf{n}_{\beta\alpha} \quad$ on $\; A_{\beta\alpha}$. (5)

In this last equation, γ is the α-β interfacial tension and $\mathbf{\Sigma}_\kappa$ represents the stress tensor associated to the κ phase given by

$$\mathbf{\Sigma}_\kappa = -p_\kappa \mathbf{I} + \mu_\kappa (\nabla \mathbf{V}_\kappa + {}^{\mathrm{t}} \nabla \mathbf{V}_\kappa), \tag{6}$$

while $\mathbf{n}_{\beta\alpha}$ is the unit normal vector to the $A_{\beta\alpha}$ interface directed from the β- to the α-phase. With the notation

$$e_{\mathrm{xxx...n\ times}} = \frac{\partial^n e}{\partial x^n}, \tag{7}$$

$\mathbf{n}_{\beta\alpha}$ can be expressed as

$$\mathbf{n}_{\beta\alpha} = (-e_x \, \mathbf{e_x} - \mathbf{e_r})/(1 + e_x^2)^{1/2}, \tag{8}$$

in the cylindrical system of coordinates ($\mathbf{e_x}$, $\mathbf{e_r}$). The algebraic double mean curvature, H, of $A_{\alpha\beta}$ is given by

$$H = e_{xx}/(1 + e_x^2)^{3/2} + 1/(R_0 - e)(1 + e_x^2)^{1/2}. \tag{9}$$

• *β-phase (free water):*
– mass balance

$$\nabla.\mathbf{V}_\beta = 0, \tag{10}$$

– momentum balance

$$0 = -\nabla p_\beta + \mu_\beta \nabla^2 \mathbf{V}_\beta. \tag{11}$$

• *β-σ interface ($r = R_0$):*

B.C. 3 $\quad \mathbf{V}_\beta = 0 \quad$ on $\; A_{\beta\sigma}$. (12)

We are now in position to derive the velocity fields in both phases and to do so we first make use of the lubrication approximation.

2.1.1. *Lubrication Approximation*

In this paragraph, we assume that velocities in the α- and β-phase are essentially directed along the tube axis and that the component along $\mathbf{e}_\mathrm{r}$ is negligible i.e.

$$\mathbf{V}_\kappa = u_\kappa \mathbf{e_x}, \qquad \kappa = \alpha, \beta. \tag{13}$$

This hypothesis is a very classical one in the study of film-flow (Landau and Levich, 1942; Bretherton, 1961) and the problem to be solved can be simplified to

• *α-phase (gas):*

$$\frac{\partial u_\alpha}{\partial x} = 0, \tag{14}$$

$$\frac{\partial p_\alpha}{\partial r} = 0, \tag{15}$$

$$\frac{\partial p_\alpha}{\partial x} = \frac{\mu_\alpha}{r}\frac{\partial}{\partial r}\left(r\frac{\partial u_\alpha}{\partial r}\right). \tag{16}$$

• *α-β interface ($r = R_0 - e(x)$):*

B.C. 4 $\quad u_\alpha = u_\beta, \quad$ on $A_{\beta\alpha}$, (17)

B.C. 5 $\quad p_\alpha - p_\beta = \gamma H, \quad$ on $A_{\beta\alpha}$, (18)

B.C. 6 $\quad \mu_\beta \dfrac{\partial u_\beta}{\partial r} - \mu_\alpha \dfrac{\partial u_\alpha}{\partial r} = 0, \quad$ on $A_{\beta\alpha}$. (19)

These two last boundary conditions result from B.C. 2 post-multiplied by $\mathbf{n}_{\beta\alpha}$ and the tangential unit vector, $\mathbf{t}_{\beta\alpha}$, respectively whereas H in B.C. 5 is still given by Equation (9).

• *β-phase (free water):*

$$\frac{\partial u_\beta}{\partial x} = 0, \tag{20}$$

$$\frac{\partial p_\beta}{\partial r} = 0, \tag{21}$$

$$\frac{\partial p_\beta}{\partial x} = \frac{\mu_\beta}{r}\frac{\partial}{\partial r}\left(r\frac{\partial u_\beta}{\partial r}\right). \tag{22}$$

• *β-σ interface ($r = R_0$):*

B.C. 7 $\quad u_\beta = 0, \quad$ on $A_{\beta\sigma}$. (23)

After integrating the above set of differential equations and making use of the axial symmetry and boundary conditions B.C. 4, B.C. 6, B.C. 7, one finds the local longitudinal gas and liquid velocities to be

$$\begin{aligned} u_\alpha \;=\; & \frac{1}{4\mu_\alpha}\frac{\mathrm{d}p_\alpha}{\mathrm{d}x}\Bigg[r^2 + 2R_0^2 \times \\ & \times (1-\tilde{e})^2\left(\frac{\mu_\alpha}{\mu_\beta}\ln(1-\tilde{e}) - \frac{1}{2}\right)\Bigg] + \qquad 0 \leqslant r \leqslant R_0(1-\tilde{e}) \\ & + \frac{1}{4\mu_\beta}\frac{\mathrm{d}p_\beta}{\mathrm{d}x}R_0^2[(1-\tilde{e})^2 - 1 - 2(1-\tilde{e})^2\ln(1-\tilde{e})], \end{aligned} \tag{24}$$

and

$$u_\beta = \frac{1}{4\mu_\beta}\frac{\mathrm{d}p_\beta}{\mathrm{d}x}\left[r^2 - R_0^2 - 2R_0^2(1-\tilde{e})^2 \ln\frac{r}{R_0}\right] + \qquad R_0(1-\tilde{e}) \leqslant r \leqslant R_0$$
$$+ \frac{1}{2\mu_\beta}\frac{\mathrm{d}p_\alpha}{\mathrm{d}x}R_0^2(1-\tilde{e})^2 \ln\frac{r}{R_0}, \tag{25}$$

where $\tilde{e}$ stands for the film thickness made dimensionless by R_0. It is important to point out here that pressure gradients are directed along the tube axis.

Because both phases were considered as viscous ones (see B.C. 6), viscous coupling through the interface appears in the above result. Furthermore, as can be seen from B.C. 5 and Equation (9), we have accepted two different pressure gradients in the α- and β-phase respectively, yielding a non-zero capillary pressure gradient and this is possible only if a film thickness gradient exists along the tube axis. Such a gradient might seem however incompatible with the lubrication approximation since the radial velocity can not be zero in this case. However, the lubrication approximation should remain valid, provided the gradient of the film thickness is small, and this point is now made clear by developing a two dimensional solution in the limit of $L_0 \gg R_0$.

2.1.2. *Two-Dimensional Solution*

In this paragraph, we present an approximated two-dimensional solution of the set of Equations (2)–(12) obtained from an asymptotic development based on the following small parameter

$$\varepsilon = \frac{R_0}{L_0}. \tag{26}$$

These equations are restated with dimensionless variables and asymptotic developments of velocities and pressures are then inserted. Doing so leads to a succession of problems at increasing order in ε. The solution of these problems up to first order are readily obtained by analytical integration (see Appendix 1). In the limit of a first order approximation in R_0/L_0, one exactly obtains the same results than using a lubrication approach (Equations 24–25); this clearly indicates that the approach developed here remains valid provided the dimensionless film thickness gradient in the tube is small compared to unity.

Bearing in mind this last major feature concerning a nearly zero film thickness gradient, the above results are employed to derive an analytical expression of liquid and gas filtration velocities in a network of capillaries and thus to derive an estimation of relative permeabilities during 1D momentum transfer in a capillary porous medium.

2.2. EXTENSION TO A NETWORK OF PARALLEL CAPILLARIES

In this section, we shall progress to our final goal by extending the above results to the case of a model porous medium made of a bundle of straight and parallel capillaries of circular cross section. The final goal is to propose an approximated but physically justified estimation of relative permeabilities for subsequent use in a computational model of drying applied on a porous medium that can be reasonably identified to a capillary network model.

2.2.1. *Filtration Velocities*

We consider here the case of a bundle made of straight and parallel capillaries of circular cross section of radius R_0 as a model of porous medium. In order to estimate filtration velocities in both phases, we keep the hypothesis that the wetting -liquid- phase is distributed under the form of films while the non-wetting one flows through the center of the tubes. The relevance of such a representation for the porous medium as well as the assumption on phase distribution will be commented afterwards while applying the model to the drying of a natural porous material. According to the phase distribution assumption, filtration velocities $\overline{\mathbf{V}}_\alpha$ and $\overline{\mathbf{V}}_\beta$ in both phases in this configuration directly follows from the above local velocity expressions by simply taking the averaged forms

$$\overline{\mathbf{V}}_\alpha = \overline{u}_\alpha \mathbf{e}_\mathbf{x} + \overline{v}_\alpha \mathbf{e}_\mathbf{r} = \phi \frac{2}{R_0^2} \int_0^{R_0(1-\tilde{e})} \mathbf{V}_\alpha r \, \mathrm{d}r, \tag{27}$$

$$\overline{\mathbf{V}}_\beta = \overline{u}_\beta \mathbf{e}_\mathbf{x} + \overline{v}_\beta \mathbf{e}_\mathbf{r} = \phi \frac{2}{R_0^2} \int_{R_0(1-\tilde{e})}^{R_0} \mathbf{V}_\beta r \, \mathrm{d}r, \tag{28}$$

where ϕ is the average porosity of the bundle of capillaries. This yields:

$$\begin{aligned} \bar{u}_\alpha \;=\; & \phi \frac{R_0^2}{8} \frac{1}{\mu_\alpha} \left(\frac{\mathrm{d}p_\alpha}{\mathrm{d}x} \right) \left[-(1-\tilde{e})^4 + 4 \frac{\mu_\alpha}{\mu_\beta} (1-\tilde{e})^4 \ln(1-\tilde{e}) \right] + \\ & + \phi \frac{R_0^2}{8} \frac{1}{\mu_\beta} \left(\frac{\mathrm{d}p_\beta}{\mathrm{d}x} \right) 2[(1-\tilde{e})^4 - (1-\tilde{e})^2 - \\ & - 2(1-\tilde{e})^4 \ln(1-\tilde{e})], \end{aligned} \tag{29}$$

$$\begin{aligned} \bar{u}_\beta \;=\; & \phi \frac{R_0^2}{8} \frac{1}{\mu_\beta} \left(\frac{\mathrm{d}p_\beta}{\mathrm{d}x} \right) [1 - (1-\tilde{e})^4 - 2((1-\tilde{e})^2 - 1)^2 + \\ & + 4(1-\tilde{e})^4 \ln(1-\tilde{e})] + \\ & + \phi \frac{R_0^2}{8} \frac{1}{\mu_\beta} \left(\frac{\mathrm{d}p_\alpha}{\mathrm{d}x} \right) 2[-(1-\tilde{e})^2 - \\ & - 2(1-\tilde{e})^4 \ln(1-\tilde{e}) + (1-\tilde{e})^4]. \end{aligned} \tag{30}$$

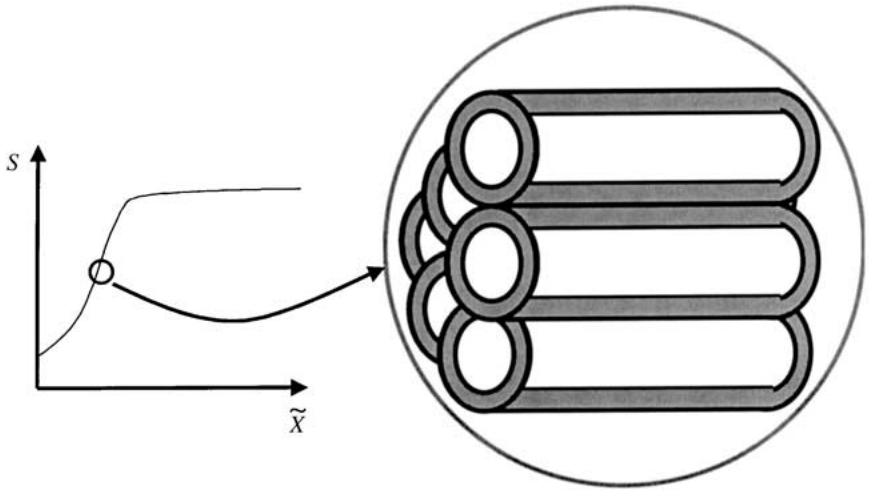

Figure 2. Local equivalent medium of the real porous medium: bundle of straight capillaries in which film thickness is constant.

In these expressions, we have deliberately kept the film thickness under its dimensionless form and this is justified by the fact that this flow model will be further employed to derive permeability- saturation relationships.

Before doing so we must be clear about the up-scaling process adopted here: the solution of the boundary value problem presented in Section 2.1. has been obtained in a capillary tube for a nearly zero local film-thickness gradient. This solution is locally used hereunder in order to describe two-phase flow in a real porous medium. With this goal in view, this real porous medium is described, at the pore scale, by a bundle of straight and parallel capillaries of circular cross section of radius R_0, the film thickness gradients in this bundle being considered as insignificant (see Figure 2). Doing so, the film flow solution we derived in Section 2.1. by using an arbitrary but physically reasonable phase distribution assumption (free water under the form of wetting films and gas phase in the center of the tubes) is only used to obtain the relationships between relative permeabilities and local water saturation. Then, neglecting free water retained in pendular rings or entrapped clusters, this local and nearly constant non-dimensional film thickness $\tilde{e}$ in a bundle of capillaries is related with the local saturation in the real porous medium by using the following coherent relationship

$$S(x) = \frac{\pi R_0^2 - \pi (R_0 - R_0 \tilde{e}(x))^2}{\pi R_0^2} = 1 - (1 - \tilde{e}(x))^2, \tag{31}$$

or equivalently

$$\tilde{e}(x) = 1 - (1 - S(x))^{1/2}. \tag{32}$$

2.2.2. *Relative Permeabilities*

At this point, our interest is to derive an estimation of relative permeabilities for the two-phase flow considered in this paper. To do so, we choose to identify these terms from the classical macroscopic model of two-phase flow in homogeneous porous media. If one believes body force to be negligible, two-phase displacement at Darcy's scale is described by a linear relation between filtration velocities and macroscopic pressure gradients in each phase (Whitaker, 1986; Auriault, 1987; Lasseux *et al*., 1996)

$$\overline{\mathbf{V}}_\alpha = -\frac{\mathbf{K}.\mathbf{K}_{r\alpha}}{\mu_\alpha} \cdot \nabla \overline{p}_\alpha^\alpha - \frac{\mathbf{K}.\mathbf{K}_{r\alpha\beta}}{\mu_\beta} \cdot \nabla \overline{p}_\beta^\beta, \tag{33}$$

$$\overline{\mathbf{V}}_\beta = -\frac{\mathbf{K}.\mathbf{K}_{r\beta}}{\mu_\beta} \cdot \nabla \overline{p}_\beta^\beta - \frac{\mathbf{K}.\mathbf{K}_{r\beta\alpha}}{\mu_\alpha} \cdot \nabla \overline{p}_\alpha^\alpha. \tag{34}$$

In these expressions, $\mathbf{K}$ represents the intrinsic permeability tensor, $\mathbf{K}_{r\kappa}$ is the relative permeability tensor to the κ-phase and $\mathbf{K}_{r\kappa\xi}$ the coupling permeability tensor between the κ-phase and the ξ-phase resulting from viscous drag at the κ-ξ interfaces. A direct identification of gas and liquid filtration velocities in Equations (29) and (30) with the x components of Equations (33) and (34) provides the effective permeabilities in the direction of the tube axis which in the present case are

$$K K_{r\beta} = \frac{R_0^2\phi}{8}[\tilde{e}(2-\tilde{e})(1-3(1-\tilde{e})^2) - 4(1-\tilde{e})^4 \ln(1-\tilde{e})], \tag{35}$$

$$K K_{r\alpha} = \frac{R_0^2\phi}{8}(1-\tilde{e})^4 \left[1 - 4\frac{\mu_\alpha}{\mu_\beta}\ln(1-\tilde{e})\right], \tag{36}$$

$$K K_{r\beta\alpha} = \frac{R_0^2\phi}{8} 2\frac{\mu_\alpha}{\mu_\beta}(1-\tilde{e})^2[\tilde{e}(2-\tilde{e}) + 2(1-\tilde{e})^2 \ln(1-\tilde{e})], \tag{37}$$

$$K K_{r\alpha\beta} = \frac{R_0^2\phi}{8} 2(1-\tilde{e})^2[\tilde{e}(2-\tilde{e}) + 2(1-\tilde{e})^2 \ln(1-\tilde{e})]. \tag{38}$$

Since the intrinsic permeability of the bundle of straight and parallel capillary tubes of radius R_0 on which these results were obtained is simply

$$K = \frac{R_0^2\phi}{8}, \tag{39}$$

the relative and coupling permeabilities can be expressed in terms of the free water saturation S by making use of Equation (31) and this yields

$$K_{r\beta} = S(3S-2) - 2(1-S)^2 \ln(1-S), \tag{40}$$

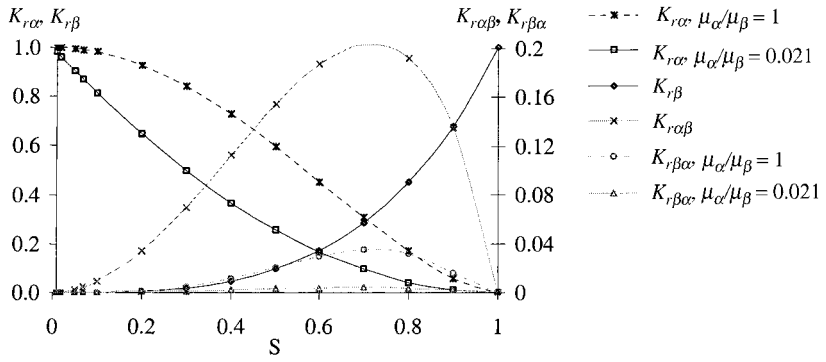

Figure 3. Relative and coupling permeabilities versus free water saturation.

$$K_{r\alpha} = (1-S)^2\left(1 - 2\frac{\mu_\alpha}{\mu_\beta}\ln(1-S)\right), \tag{41}$$

$$K_{r\beta\alpha} = 2\frac{\mu_\alpha}{\mu_\beta}(1-S)(S + (1-S)\ln(1-S)), \tag{42}$$

$$K_{r\alpha\beta} = 2(1-S)(S + (1-S)\ln(1-S)). \tag{43}$$

These results are in complete agreement with expressions obtained under a similar physical situation where a longitudinal slow flow of two incompressible fluids was considered (Bacri *et al.*, 1990). Furthermore, these permeability terms have the expected behavior in the limit $S=0$ or $S=1$ as can be seen in Figure 3 where we have represented the four permeability terms versus free water saturation for two values of the viscosity ratio μ_α/μ_β. The viscosity ratio - $\mu_\alpha/\mu_\beta = 0.021$ – corresponds to the air-water viscosity ratio used to simulate our experiments.

Although they intimately depend on the configuration and set of hypotheses under consideration here, three important features must be outlined from the results in this figure. First, as expected, relative permeabilities are independent of the tube radius, R_0. Secondly, relative permeability to the non-wetting phase as well as β-α coupling relative permeability are strongly affected by the viscosity ratio of the two phases – while the two other ones are not. Thirdly, in this particular case, viscous coupling – especially in the α-phase – can be significant in comparison to the corresponding relative permeability term and this raises the question of the relevance of viscous coupling for multi-phase flow in porous media. It is beyond the scope of this paper to discuss that particular point thoroughly (see a review on this topic by Ayub and Bentsen, 1999), and in the following the classical approach for which coupling is neglected will be considered, corresponding to the classical generalized two-phase Darcy's law.

In the next section, relative permeabilities derived above -and only these quantities- are inserted into a numerical model developed elsewhere (Couture, 1995) in

order to describe free water transfer in the non-hygroscopic region – $0 \leqslant S \leqslant 1$ – during drying of a particular capillary porous medium. All other thermo-physical characteristics were taken from experimental measurements on oak wood.

3. Application to Longitudinal Drying of Oak Wood

The relative permeabilities calculated above were used to perform one-dimensional numerical simulations of convective drying of a capillary porous medium in the non-hygroscopic region. As a validation test of the phenomenology under question in this work, computational results will be further compared with experimental ones. In order to keep some coherence with the bundle of capillary tubes model assumed previously, we chose to perform this comparison for the case of longitudinal drying of a sample of oak wood. The structure of this type of wood has been analyzed in details (Siau, 1984). It is essentially composed of cellulose, hemi-cellulose and lignin. Cellulose is the skeleton of the wood while hemi-cellulose is the matrix. Lignin, the encrusting substance, binds cells together and gives rigidity to the cell walls. Anatomy of oak clearly shows the major existence of vessels in fibers direction justifying that a parallel capillary tubes analogy, even if extreme, is however reasonable. Moreover, physical properties of oak are rather well characterized (Hernandez, 1991) (see Table I) and this further motivated our choice.

If one is willing to use a model of capillary tubes to represent the actual porous medium, some equivalence criteria must be selected to keep the essential features of the medium regarding the physical process under concern. This problem has been addressed in the literature (Dullien, 1979; Ehrlich *et al.*, 1991) and it is beyond the scope of this work to discuss thoroughly the details of such a task. We simply assume here that the equivalence in terms of average porosity, intrinsic permeability and capillary pressure function is sufficient to capture the essential properties of this type of material for the longitudinal drying process.

3.1. PHYSICAL AND NUMERICAL MODEL

The physical model is based on heat, mass and momentum transport at Darcy's scale as obtained by volume averaging the corresponding pore scale balance equations (Whitaker, 1977). In order to obtain a well posed problem and a convenient discrete form for the numerical treatment, the conservative set of equations is written as

- *species mass balance:*
  – dry air

$$\frac{\partial \overline{\rho}_{\mathrm{a}}}{\partial t} + \nabla.(\overline{\rho}_{\mathrm{a}}^{\alpha}\overline{\mathbf{V}}_{\mathrm{a}}) = 0, \tag{44}$$

Table I. Physical characteristics of oak wood

Physical characteristics of oak wood obtained by direct measurements (Hernandez, 1991)		
D_b	Bound water diffusivity ($m^2\,s^{-1}$)	0 if $W > W_{sp}$ else $\frac{2.5}{\overline{\rho}_s}\exp\left[\left(\frac{10886.472}{\overline{T}}\right)W - \frac{7600.75}{\overline{T}} + 6.8\right]$
D_v^{eff}	Diffusivity of vapor in gas ($m^2\,s^{-1}$)	$50 \times B(\phi)\left(8.9210^{-5}\frac{\overline{T}^{1.81}}{\overline{p}_g^{-g}}\right)$ $B(\phi) = \frac{\phi^6}{20}$
$p_c(S)$	Capillary pressure (Pa) (See Appendix)	$1/p_c(S) = 3.895 \times 10^{-3} + 94.69 \times 10^{-3} \cdot S$ $-0.895 \cdot S^2 + 8.155 \cdot S^3 - 33.96 \cdot S^4 + 68.10 \cdot S^5$
S_{irr}	Irreducible saturation	0.4
W_{ini}	Initial dry based moisture content	0.86
W_{sp}	Dry based moisture content at the saturation point	0.4
ϕ	Porosity	0.5
ρ	Density ($kg.m^{-3}$)	1000
$\overline{\rho_\sigma}$	Solid density ($kg.m^{-3}$)	750
λ	Effective thermal conductivity ($W.m^{-1}.K^{-1}$)	$2.5 \times (0.386W + 0.137)$
Physical characteristics of oak wood coming from the literature (Siau, 1984)		
a_w	Water activity (-)	Bradley's model (1936) 1 if $W > W_{sp}$ $\exp\left(-AB^{100W} + C\right)$ if $W \leqslant W$sp $A = 2.51 \times 10^{-4}\overline{T}^2 + 0.1780\,\overline{T} + 35.719$ $B = -9.475 \times 10^{-4}\overline{T} + 1.133$ $C = 0$
K	Intrinsic permeability (m^2)	3×10^{-15}

– water

$$\frac{\partial W}{\partial t} + \nabla.\left\{\frac{1}{\overline{\rho}_\sigma}(\overline{\rho}_\beta^\beta\overline{\mathbf{V}}_\beta + \overline{\rho}_v^\alpha\overline{\mathbf{V}}_v + \overline{\rho_b\mathbf{V}_b})\right\} = 0. \tag{45}$$

• *momentum balance:*

– free water

$$\begin{aligned}&\overline{\rho}_\beta^\beta \overline{\mathbf{V}}_\beta = \overline{\rho}_\beta^\beta \frac{K K_{r\beta}}{\mu_\beta} \nabla p_{\mathrm{c}} - \overline{\rho}_\beta^\beta \frac{K K_{r\beta}}{\mu_\beta} \nabla \overline{p}_\alpha^\alpha, \quad \text{if } W > W_{\mathrm{sp}},\\ &\overline{\rho}_\beta^\beta \overline{\mathbf{V}}_\beta = 0, \quad \text{if } W \leqslant W_{\mathrm{sp}}.\end{aligned} \tag{46}$$

– bound water

$$\begin{cases} \overline{\rho_{\mathrm{b}} \mathbf{V}_{\mathrm{b}}} = 0, \quad \text{if } W > W_{\mathrm{sp}}, \\ \overline{\rho_{\mathrm{b}} \mathbf{V}_{\mathrm{b}}} = -\overline{\rho}_\sigma D_{\mathrm{b}} \nabla W, \quad \text{if } W \leqslant W_{\mathrm{sp}}. \end{cases} \tag{47}$$

– vapor

$$\overline{\rho}_{\mathrm{v}}^\alpha \overline{\mathbf{V}}_{\mathrm{v}} = \overline{\rho}_{\mathrm{v}}^\alpha \frac{K K_{r\alpha}}{\mu_\alpha} \nabla \overline{p}_\alpha^\alpha - \overline{\rho}_\alpha^\alpha D_v^{\mathrm{eff}} \nabla C, \tag{48}$$

– dry air

$$\overline{\rho}_{\mathrm{a}}^\alpha \overline{\mathbf{V}}_{\mathrm{a}} = \overline{\rho}_{\mathrm{a}}^\alpha \frac{K K_{r\alpha}}{\mu_\alpha} \nabla \overline{p}_\alpha^\alpha + \overline{\rho}_\alpha^\alpha D_{\mathrm{v}}^{\mathrm{eff}} \nabla C, \tag{49}$$

where C is the vapor mass fraction defined as

$$C = \frac{\overline{\rho}_{\mathrm{v}}}{\overline{\rho}_\alpha}. \tag{50}$$

• *energy balance (one-temperature model):*

$$\begin{aligned}\frac{\partial \overline{H}}{\partial t} \; + \; \nabla . &\left\{ \begin{array}{l} (\overline{\rho}_\beta^\beta \overline{\mathbf{V}}_\beta C_{\mathrm{p}_\beta} + \overline{\rho_{\mathrm{b}} \mathbf{V}_{\mathrm{b}}} C_{\mathrm{p}_\beta} + \overline{\rho}_{\mathrm{a}}^\alpha \overline{\mathbf{V}}_{\mathrm{a}} C_{\mathrm{p_a}} + \overline{\rho}_{\mathrm{v}}^\alpha \overline{\mathbf{V}}_{\mathrm{v}} C_{\mathrm{p_v}}) \overline{\mathrm{T}} \\ + h_{\mathrm{v}}^0 \overline{\rho}_{\mathrm{v}}^\alpha \overline{\mathbf{V}}_{\mathrm{v}} + h_{\mathrm{b}} (\overline{\rho}_\beta^\beta \overline{\mathbf{V}}_\beta + \overline{\rho}_{\mathrm{v}}^\alpha \overline{\mathbf{V}}_{\mathrm{v}}) - \lambda \nabla \overline{T} \end{array} \right\} \\ &= (\overline{\rho}_\beta^\beta \overline{\mathbf{V}}_\beta + \overline{\rho}_{\mathrm{v}}^\alpha \overline{\mathbf{V}}_{\mathrm{v}} + \overline{\rho_{\mathrm{b}} \mathbf{V}_{\mathrm{b}}}) \cdot \nabla h_{\mathrm{b}}. \end{aligned} \tag{51}$$

In this last equation, h_{v}^0 and h_{b} are the latent heat of vaporization at the reference temperature – $T = 273K$ – and heat of desorption respectively while $\overline{H}$ represents the mean enthalpy of the system

$$\overline{H} = \overline{\rho C_{\mathrm{p}} T} \tag{52}$$

with

$$\overline{\rho C_{\mathrm{p}}} = \overline{\rho}_\sigma C_{\mathrm{p}_\sigma} + (\overline{\rho}_\beta^\beta + \overline{\rho}_{\mathrm{b}}) C_{\mathrm{p}_\beta} + \overline{\rho}_{\mathrm{v}} C_{\mathrm{p_v}} + \overline{\rho}_{\mathrm{a}} C_{\mathrm{p_a}}. \tag{53}$$

To this set of equations, one must add the relevant boundary conditions at the surface of the sample for the process under study. For convective drying, and with the choice made above for the conservation equations, they can be stated as follows

• *dry air density*: the boundary condition is a Dirichlet condition

$$\overline{\rho}_{\mathrm{a}} = \frac{M_{\mathrm{a}} \varepsilon_\alpha}{RT} (p_{\mathrm{amb}} - \overline{p}_{\mathrm{v}}^\alpha), \tag{54}$$

where M_a is the molar mass of air, R is ideal gas constant, p_{amb} is the ambient pressure and $\overline{p}_{\mathrm{v}}^{\alpha}$ is the partial vapor pressure in the drying air and is related to the saturation pressure $\overline{p}_{\mathrm{v\,sat}}^{\alpha}$ at the corresponding temperature

$$\overline{p}_{\mathrm{v}}^{\alpha} = a_{\mathrm{w}} \overline{p}_{\mathrm{v\,sat}}^{\alpha}, \tag{55}$$

with a_{w} the water activity.

• *water content:* this condition is a Neumann condition and results from the mass flux continuity at the surface of the sample

$$\left\{ \frac{1}{\overline{\rho}_{\sigma}} (\overline{\rho}_{\beta}^{\beta} \overline{\mathbf{V}}_{\beta} + \overline{\rho}_{\mathrm{v}}^{\alpha} \overline{\mathbf{V}}_{\mathrm{v}} + \overline{\rho_{\mathrm{b}} \mathbf{V}_{\mathrm{b}}}) \right\} \cdot \mathbf{n} = \frac{F_{\mathrm{m}}}{\overline{\rho}_{\sigma}}, \tag{56}$$

$\mathbf{n}$ being the outwardly directed unit normal vector and with F_{m} given by:

$$F_{\mathrm{m}} = h_{\mathrm{m}} (\overline{\rho}_{\mathrm{v}}^{\alpha} - \rho_{\mathrm{v\,amb}}), \tag{57}$$

h_{m} being the mass exchange coefficient which can be identified from the heat exchange coefficient, h_{T}, (see Equation (59)) with a Lewis analogy (Lewis, 1921) and $\rho_{\mathrm{v\,amb}}$ the vapor density under ambient conditions.

• *enthalpy:* a Neumann type boundary condition is also employed to express the heat flux continuity

$$\begin{aligned} &\left\{ \begin{array}{l} (\overline{\rho}_{\beta}^{\beta} \overline{\mathbf{V}}_{\beta} C_{\mathrm{p}\beta} + \overline{\rho_{\mathrm{b}} \mathbf{V}_{\mathrm{b}}} C_{\mathrm{p}\beta} + \overline{\rho}_{\mathrm{a}}^{\alpha} \overline{\mathbf{V}}_{\mathrm{a}} C_{\mathrm{pa}} + \overline{\rho}_{\mathrm{v}}^{\alpha} \overline{\mathbf{V}}_{\mathrm{v}} C_{\mathrm{pv}}) \overline{T} \\ + h_{\mathrm{v}}^{0} \overline{\rho}_{\mathrm{v}}^{\alpha} \overline{\mathbf{V}}_{\mathrm{v}} + h_{\mathrm{b}} (\overline{\rho}_{\beta}^{\beta} \overline{\mathbf{V}}_{\beta} + \overline{\rho}_{\mathrm{v}}^{\alpha} \overline{\mathbf{V}}_{\mathrm{v}}) - \lambda \nabla \overline{T} \end{array} \right\} \cdot \mathbf{n} \\ &\qquad = Q + (h_{\mathrm{v}}^{0} + h_{\mathrm{b}} + C_{p_{\mathrm{v}}} \overline{T}) F_{\mathrm{m}} + (\overline{\rho}_{\mathrm{a}}^{\alpha} \overline{\mathbf{V}}_{\mathrm{a}} C_{p_{\mathrm{a}}} \overline{T}) \cdot \mathbf{n}, \end{aligned} \tag{58}$$

where

$$Q = h_{\mathrm{T}} (\overline{T} - T_{\mathrm{amb}}), \tag{59}$$

represents the total heat flux at the sample surface. In this last equation, the heat exchange coefficient, h_{T}, is determined experimentally from the isenthalpic phase of drying. In fact, during this phase, it is classically admitted that the evaporation front is located at the upper surface of the material and that heat loss due to evaporation is exactly compensated by the convective heat supply.

Under this form, the system of coupled equations can be solved for $\overline{\rho}_{\mathrm{a}}$, $\overline{H}$, and W using a finite element method and a semi-implicit time integration scheme.

3.2. RESULTS OF DRYING NUMERICAL SIMULATIONS

The numerical model employed here was developed to simulate drying of a non-shrinkable hygroscopic capillary porous medium (Couture *et al.*, 1996). For our one-dimensional simulations, we introduced the relative permeabilities obtained in Equations (81) and (82) as well as physical characteristics of the oak wood

(see Table 1) employed for the experiments presented in Section 4. Because of its heterogeneous and variable character, this material exhibits structural and chemical variability as reflected by its physical properties found in the literature such as permeability, capillary pressure, thermal conductivity and diffusivity of bound water. Characteristics given in Table 1 were either obtained by direct measurements in our laboratory (Hernandez, 1991) or/and taken from the literature (Siau, 1984).

Intrinsic data like porosity, permeability and capillary pressure function used in our simulations were measured on dry samples of oak wood. These data basically depend on the microscopic morphology of the material and it is well known that drying of such a hygroscopic medium yields a significant shrinkage (Nadeau and Puiggali, 1995). For this reason, it might seem a crude approximation to use these data in drying simulations of the material initially partially water-saturated. A short discussion of the physical relevance of the use of such data for our simulation is proposed in Appendix 2.

Our numerical simulations were performed under the same convective drying conditions and initial state – $W_{ini} = 0.86$ – and the same sample dimensions as the ones used for the experiments detailed below. The sample has only one open end subjected to the convective drying flux so that drying is a longitudinal 1D process. In addition, it is assumed to be homogeneous. For direct comparison with experimental data, the main result is in terms of the evolution of the profiles of moisture content along the sample. This result issued from the numerical simulation is represented in Figure 4. It has to be emphasized that the film-flow model proposed here operates only in the non hygroscopic region, which, for the case under study, corresponds to local moisture contents greater than 0.4.

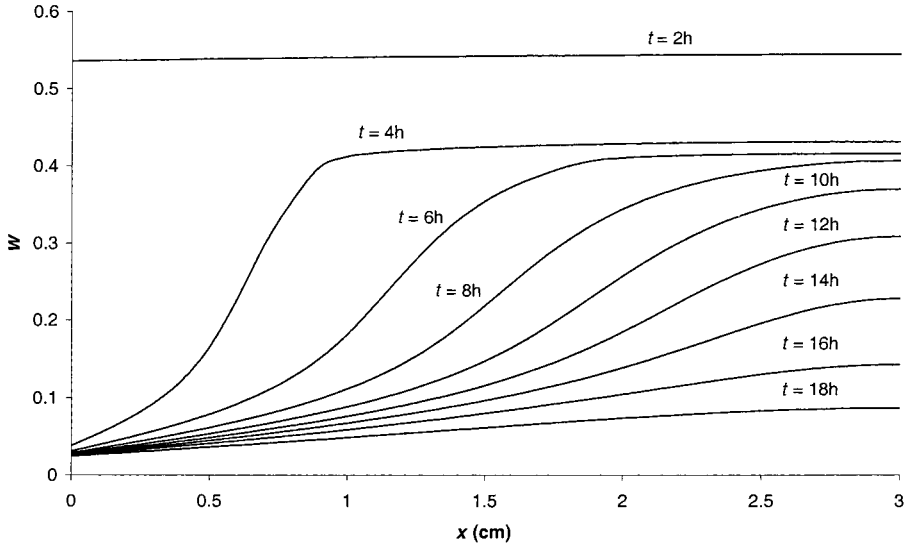

Figure 4. Evolution of the moisture content along the sample as predicted by a 1D numerical simulation including our film flow model. The drying period is from 2 h to 18 h and initial water content is 0.86 that $S_{ini} = 0.69$.

4. Comparison with Drying Experiments on Oak Wood

In order to validate the film-flow model derived in this paper, convective drying experiments were performed on oak wood.

4.1. MATERIAL AND PROCEDURE

• *Sample*
The sample is a right angle parallelepiped of pedonculate oak wood with the following dimensions

– height (longitudinal dimension): 3 cm,
– width: 3 cm,
– thickness (gamma crossed dimension, see below): 2 cm.

Before beginning the experiment, the sample is partially saturated with water by immersion during one month. Its initial dry based moisture content is $W_{\text{ini}} = 0.86$ that is $S_{\text{ini}} = 0.69$. By using the pore radius distribution measured by Hernandez in 1991 for pedonculate oak wood, and by assuming that the equivalence in terms of porosity and intrinsic permeability is sufficient to capture the essential properties of this type of material for the longitudinal drying process, it is possible to extract an equivalent uniform radius R_0. In fact, if $\Psi(\text{r})$, $R_{\min}$ and $R_{\max}$ are the pore radius distribution function, the minimum and the maximum pore radii identified on the real sample by a mercury injection process, then R_0 is given by:

$$R_0 = \left(\int_{R_{\min}}^{R_{\max}} \Psi\,(\text{r})\, r^2\, \text{d}r \right)^{1/2} . \tag{60}$$

For the oak used in this work, the pore radius distribution function has the following form (Hernandez, 1991)

$$\Psi(\text{r}) = \frac{1}{r^3} \frac{2}{1/R_{\max}^2 - 1/R_{\min}^2}, \tag{61}$$

and this leads to

$$R_0 = \left(\frac{2 \ln \dfrac{R_{\min}}{R_{\max}}}{1/R_{\max}^2 - 1/R_{\min}^2} \right)^{1/2} . \tag{62}$$

Using this last equation, and considering that capillaries of radii greater than 1 μm are concerned with free water transfer (smaller ones being filled with bound water during free water transfer), the average radius R_0 is about 3 μm. For this capillary size, the initial saturation value ($S_{\text{ini}} = 0.69$) corresponds to film thickness of about 1.35 μm. For this value, short and long range forces have a negligible

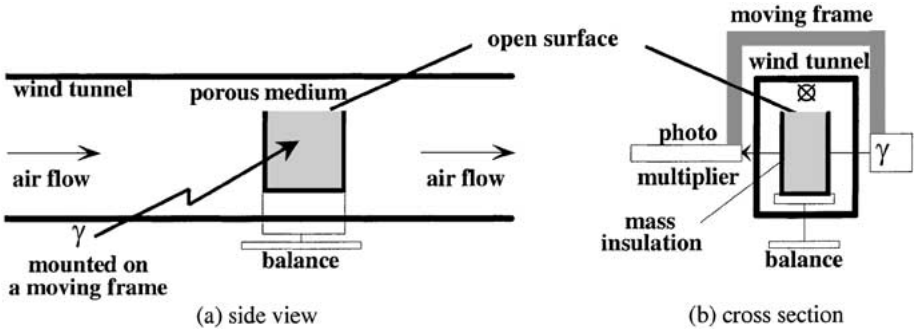

Figure 5. Drying experimental set-up.

contribution (Israelachvili, 1985) and one can postulate that such thick films can ensure capillary transfer of free water. The saturation value corresponding to a film thickness of 100 nm extracted from Equation (31) is nearly 0.06. For lower saturations, the film flow model developed above is not consistent.

In order to ensure exclusive longitudinal mass transfer during drying, all faces, except the upper one which is left opened, are insulated using an adequate glue (see Figure 5). The sample is placed in the tunnel with fibers aligned vertically.

• *Experimental set-up*

The experimental set-up used for the drying experiments is illustrated in Figure 5. It basically consists of a wind tunnel, where temperature and relative humidity are controlled, supplying hot air to a sample of oak wood. Moisture content measurements are performed by the means of a gamma ray attenuation method (Plumb *et al.*, 1985; Collignan, 1988; Bonneau, 1991; Couture *et al.*, 1996). The gamma ray attenuation system is made of a 450 mCi ^{241}Am-source and a detector composed of a NaI scintillating crystal associated to a photo multiplier tube. The gamma ray was collimated with a slit of 1 mm in height and 6 mm in width so that the measurement is actually an averaged value of the moisture content over a 1 mm × 6 mm × 20 mm volume. The source and detector are mounted on a common two-dimensional moving frame (see Figure 5(b)) displaced with a step-by-step electric motor. In addition to local measurements, the total moisture content is determined by weighing the sample throughout the drying process in order to provide the global drying kinetic. To do so, the sample is placed on a holder standing on a scale during drying. Air regulation inside the tunnel, displacement of the frame, acquisition of the signal and scale are computer-monitored.

• *Procedure*

Because of mass and thermal insulation of the sample, the process is basically 1D and for this reason, profiles of moisture content were acquired along the longitudinal -vertical- sample direction. In order to observe moisture gradients along these profiles, severe drying conditions were selected. The choice of these conditions

was inspired by previous works on drying of oak wood reported in the literature (Baixeras, 1995; Guilmain, 1997), taking into account, however, that in these works, drying was performed in the transverse direction for which permeability is much smaller than the longitudinal one. Air conditions were taken as

- temperature: 80°C,
- relative humidity: 15%,
- tangential velocity relative to upper surface of the sample: 3 m/s.

With the gamma ray attenuation system, measurements can be performed along vertical sections of the porous sample at regular intervals of time. Because the period of acquisition of the gamma ray signal by the detector can be short compared to the characteristic time of the drying process – typically, the computer-monitored acquisition time is of the order of 10 s – this technique provides an accurate way of determining moisture content profiles. Nevertheless, in the present experiment, an acceptable compromise between spatial and time resolutions must be found however and this compromise can be expressed by the two following constraints:

- to keep a reasonable signal-to-noise ratio, a sufficiently long period of acquisition on the detector must be chosen. After several tests, an acquisition time of 30 s was selected in order to achieve an acceptable gamma contrast for our 2 cm-thick sample;
- the total time required to obtain a complete moisture content profile along the sample must be small enough compared to the characteristic time of moisture evolution inside the sample for the profile to be considered as an instantaneous one. However, the number of points on each profile must be large enough in order to capture the moisture gradients correctly. Since the time of displacement between two points is less than 3 s, 26 points of measurement, 1 mm apart, were set along the sample, with the first one at 5 mm from the top. This corresponds to a total time of acquisition of about 15 min for each profile. During this interval of time, the variation of the local moisture content was of the same order of magnitude than the noise on the signal and for this reason the acquisition of a complete moisture profile was chosen to be performed every 20 min.

4.2. RESULTS AND COMPARISON WITH PREDICTIONS

The aim of this paragraph is to test the ability of the film flow free water description proposed in this paper to capture the order of magnitude of free water transfer taking place in a capillary porous medium during drying. This is done by comparing the drying simulations with Darcy's scale experimental results. Simulations are performed either by using the relative permeabilities obtained at the Darcy's scale from the film flow model developed at the pore scale, or by using the empirical model of relative permeabilities developed by Couture *et al.*, for pine wood and adapted by Baixeras for oak wood.

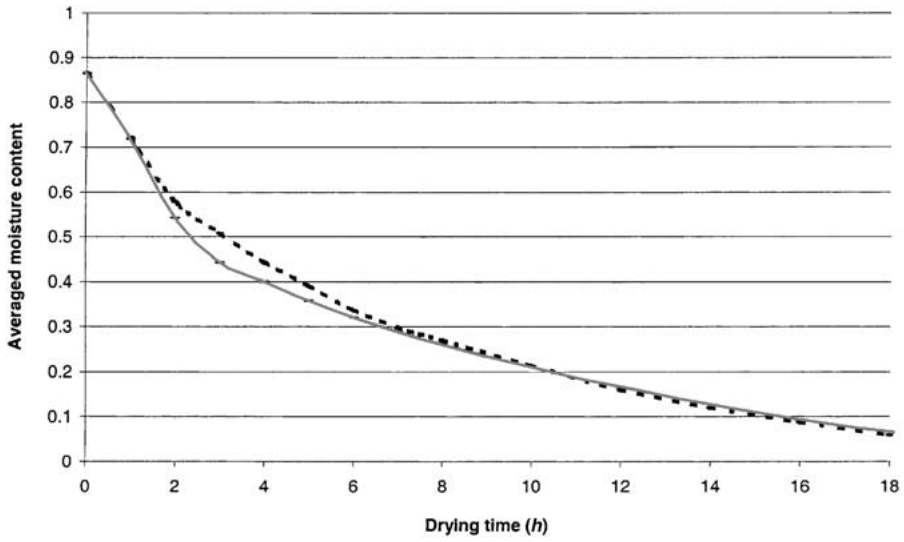

Figure 6. Comparison of experimental and predicted evolution of moisture content profiles. Continuous line represents results obtained with the film-flow model proposed in this paper while dotted line is the experimental results obtained from the gamma ray attenuation technique.

Drying of the sample took place in about 20 h with a drying kinetic represented in Figure 6. In this figure, we have reported the evolution of the average moisture content calculated by averaging profiles obtained from the gamma ray attenuation. For comparison purposes, the drying kinetic obtained from the numerical simulations using film flow relative permeabilities or empirical relative permeabilities of Baixeras were also reported.

Although agreement is quite acceptable for the overall process, a noticeable discrepancy appears for the drying period between 2 and 7 h. During this period, the predicted average moisture content is smaller than the observed one. In fact, the mass flux, which is directly proportional to the time derivative of the average moisture content, is underestimated between 2 and 3 h and overestimated between 3 and 7 h. It has to be emphasized, however, that the mass flux has not been directly taken as an adjustable parameter (see Equations (97) and (98)).

To further discuss the physical relevance of using relative permeabilities obtained from our film flow model to describe free water transfer in the non-hygroscopic region (i.e. for $W \geqslant W_{sp} = 0.4$ in the present case), a more detailed comparison between the experimental as well as the two numerical moisture content profiles along the sample is necessary (see Figure 7). Again, the agreement between the three is quite correct from a general point of view and we first focus our attention on the non-hygroscopic region of the medium – where our film flow approach is used. Although it is not the purpose of this paper, we shortly discuss the comparison in the hygroscopic region.

At the beginning of the drying – during about 1 h – most of the moisture profiles measured experimentally indicates that the entire sample remains in the so-called 'funicular zone' ($S \geqslant S_{irr} = 0.4$ i.e. $W \geqslant 0.66$) of the non-hygroscopic region ($S \geqslant 0$ i.e. $W \geqslant 0.4$). The prediction with our film-flow model and Baixeras

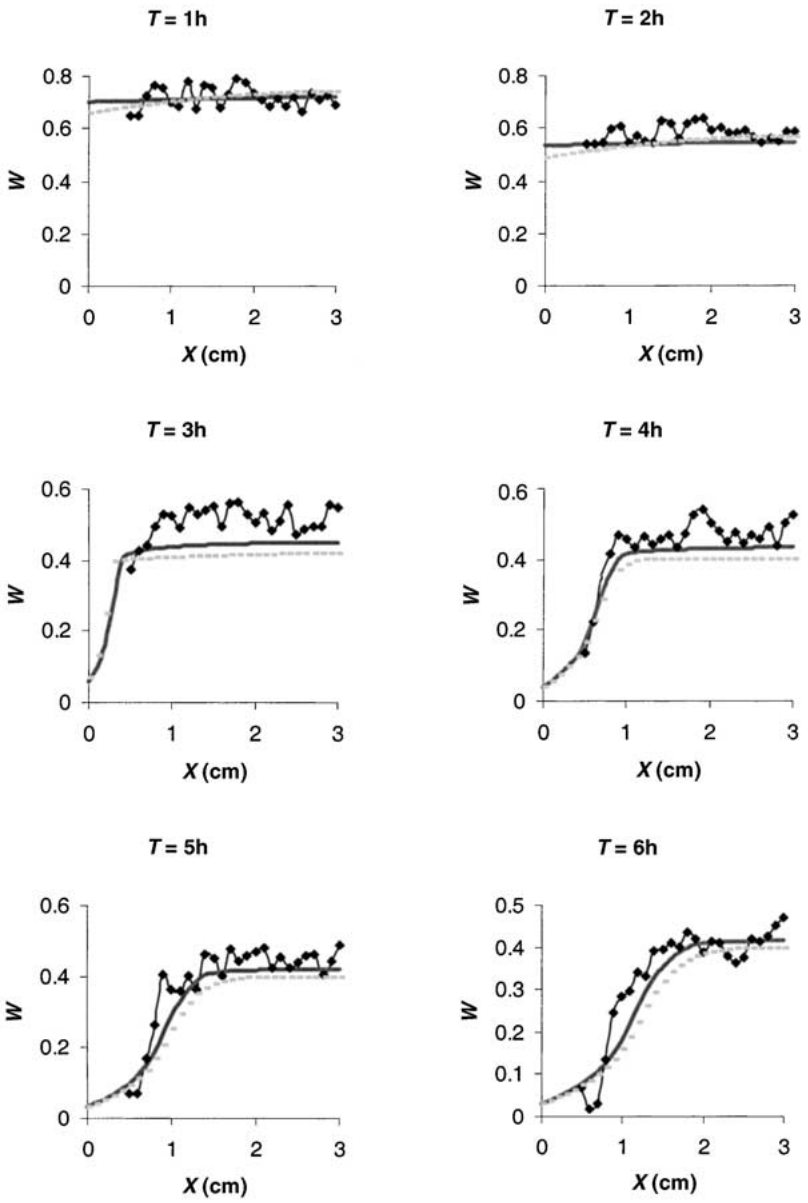

Figure 7. Comparison of experimental and predicted moisture content profiles along the sample during the longitudinal drying of oak wood (the origin of the x-axis corresponds to the open end of the sample).

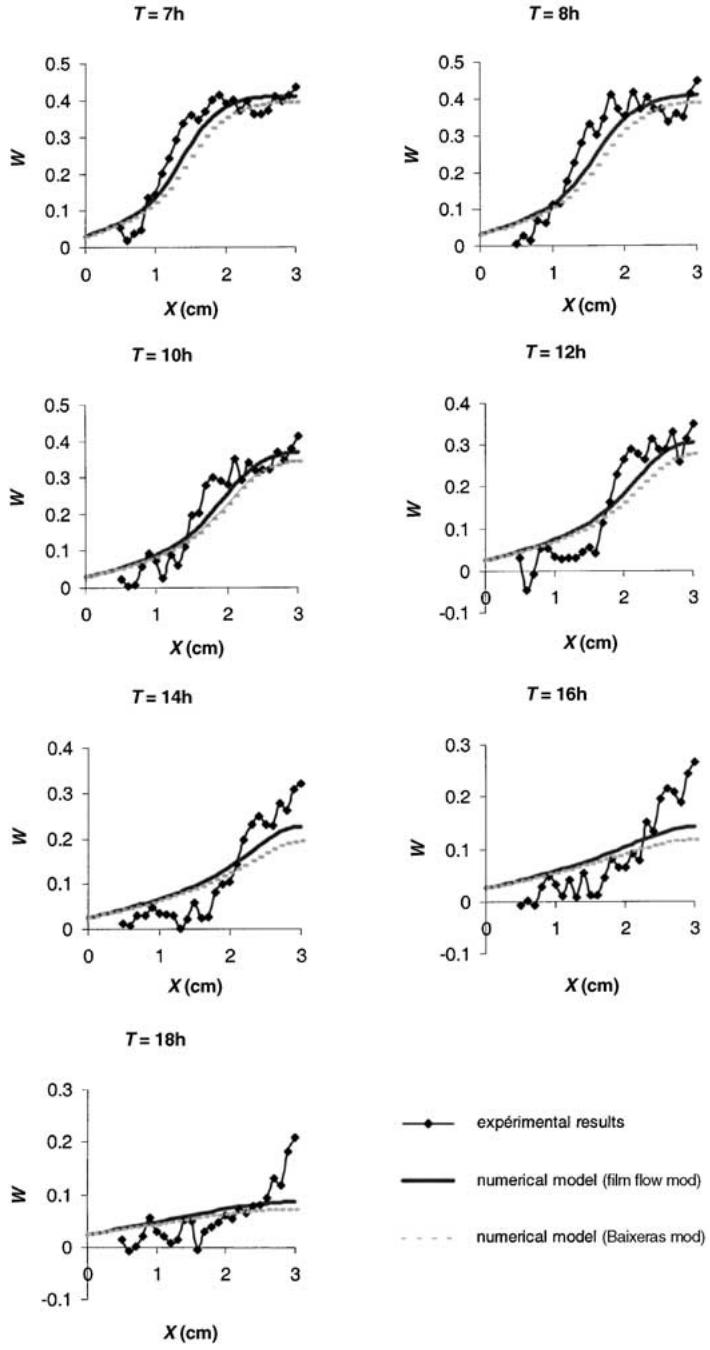

Figure 7. (*continued*)

empirical relative permeabilities perfectly reproduce the experimental observation in this region.

Between 2 and 4 h of drying, numerical results are such that the part of the sample which still remains in the non-hygroscopic region ($W \geqslant W_{sp} = 0.4$) is in the so-called 'pendular' zone ($0 \leqslant S \leqslant S_{irr} = 0.4$ i.e. $0.4 \leqslant W \leqslant 0.66$). Within this zone, numerical results indicate that moisture content quickly falls to 0.4 – which corresponds to the transition value to the hygroscopic region – in a uniform manner within less than two hours, and again, this overestimates the experimental free water transfer behavior. Note that this discrepancy is more pronounced for Baixeras empirical approach. To our opinion, this overestimation of the free water transfer by our film flow model directly follows from an overestimation of the liquid relative permeability (Equation (81)) in the pendular zone. This seems quite natural and is actually in perfect coherence with the hypothesis made for the film flow approach:

- the free liquid distribution in the pendular zone. In this zone, all the free water was assumed to be under the form of wetting liquid films which surely overestimates the saturation in these films – and consequently the liquid permeability – disregarding pendular rings and entrapped clusters;
- the thickness of free water films. In this zone, when saturation values are below 0.06, film thickness values are two small for the physics to be correctly described without taking into account the disjoining pressure.

  Between 5 and 7 h of drying numerical values of the moisture content are close to W_{sp} in the pendular zone. As a consequence, bound water transfer in the hygroscopic region ($W < W_{sp}$) strongly influences free water transport and numerical and experimental profiles are in correct agreement in the whole sample during this period. Later, discrepancy slowly increases until the end of the process but this can not be explained by relative permeability values since, at this stage all the sample is in the hygroscopic region.

  In this hygroscopic region, the following remarks can be pointed out that may explain the discrepancy between experimental and numerical evolution of moisture content (Couture *et al.*, 1996):

- the effective diffusivity of vapor in gas within the medium depends on a factor $B(\phi)$ and the estimation of this factor can have a significant influence in the transfer description in the hygroscopic region;
- the correlation used for the mass diffusivity of bound water, D_b, was derived from experimental data obtained for moisture contents ranging from 0 to 0.15. This relation was assumed to remain valid up to the saturation point value – $W_{sp} = 0.4$ – in our simulations;
- error in the profile determination using the gamma ray attenuation method increases when moisture content becomes very low (Plumb *et al.*, 1985). This has been confirmed by comparing moisture content obtained from gamma ray attenuation on the one hand and from direct mass measurements on cuttings

on the other hand (Collignan, 1988). While agreement between the two methods is excellent at high moisture levels, there is a systematic underestimation with the gamma ray attenuation technique in the hygroscopic region. This can be attributed to the fact that the gamma ray adsorption coefficient of adsorbed water might significantly differ from the one in bulk water.

5. Conclusions

In this work, we have investigated the possibility of justifying the description of drying of a capillary porous medium by extending the use of a continuous generalized Darcy's law in the pendular zone. Starting from the hypothesis that wetting films are able to maintain liquid connectivity, a simplified film-flow model of relative permeabilities was derived for two-phase flow in a bundle of cylindrical capillaries of circular cross section. Under the assumption that the wetting phase is entirely distributed in films in the pendular zone while the non-wetting phase flows in the center of the tubes, this model was used as a test to describe longitudinal drying of oak wood *without any adjustable parameter*. To do so, the bundle of capillary tubes was employed as a simplified geometrical representation of this material, keeping porosity, intrinsic permeability and capillary pressure of the natural sample. On the basis of this representation a drying numerical simulation was performed and compared to an experiment performed on an oak sample in the longitudinal direction.

Although the model proposed in this work captured the main features of the process, it was found that the liquid permeability is overestimated in the pendular zone. Even if the geometrical representation of the natural medium under consideration in this work was surely an oversimplification while estimating the relative permeabilities, this overestimation is absolutely coherent with the phase distribution assumption. In fact, due to the presence of trapped menisci – pendular rings- only a fraction of the liquid saturation should be considered as being in the films, leading to a significant reduction of the corresponding liquid relative permeability. However, no values of this fraction of the saturation are available so far and further work is required to estimate this ratio.

From a general point of view and in spite of the simplifying assumptions, the comparison between numerical and experimental results on the evolution of moisture content shows a good agreement. This brings strong arguments to confirm that

(i) a generalized Darcy's law is justified to describe the drying process in the overall non-hygroscopic region;

(ii) the film-flow model presented in this paper, even if it is oversimplified because of the local geometry assumed at the pore scale ensures a free water transfer that:

– correctly fits experimental behavior at Darcy's scale when free water saturation values are consistent with physical hypothesis retained to develop this film flow model (film-thickness greater than 100 nm);
– differs from experimental observation at this scale, when free water saturation values are too small (film-thickness smaller than 100 nm). In this range of saturation, this discrepancy can be explained by an oversimplification of the film-flow physics on the one hand and of phase distribution at the pore scale in the real medium on the other hand.

The main advantage of the film flow model presented in this paper is to provide a reasonable relative permeability prediction without any adjustable parameter leading to a correct estimation of 1D free water transfer during drying of a capillary porous medium.

Appendix 1. A Film-Flow Model in a Single Cylindrical Capillary Tube: Two-Dimensional Solution

In this appendix, we present an approximated two-dimensional solution to the set of Equations (2)–(12) obtained from an asymptotic development based on the following small parameter

$$\varepsilon = \frac{R_0}{L_0}. \tag{63}$$

Doing so requires the problem to be restated with dimensionless variables and we use $\tilde{x}$ and $\tilde{r}$ for the longitudinal and radial coordinates made dimensionless by L_0 and R_0 respectively, $\tilde{p}_\alpha$ and $\tilde{p}_\beta$ for pressures made dimensionless by γ/R_0, while $\tilde{\mathbf{V}}_\alpha$ and $\tilde{\mathbf{V}}_\beta$ are the α- and β-phase velocities of components $(\tilde{u}_\alpha, \tilde{v}_\alpha)$ and $(\tilde{u}_\beta, \tilde{v}_\beta)$ made dimensionless by γ/μ_α and γ/μ_β respectively. The two-dimensional problem is now:

• *α-phase (gas):*

$$\varepsilon \frac{\partial \tilde{u}_\alpha}{\partial \tilde{x}} + \frac{1}{\tilde{r}} \frac{\partial (\tilde{r}\tilde{v}_\alpha)}{\partial \tilde{r}} = 0, \tag{64}$$

$$\varepsilon \frac{\partial \tilde{p}_\alpha}{\partial \tilde{x}} = \varepsilon^2 \frac{\partial^2 \tilde{u}_\alpha}{\partial \tilde{x}^2} + \frac{\partial^2 \tilde{u}_\alpha}{\partial \tilde{r}^2} + \frac{1}{\tilde{r}} \frac{\partial \tilde{u}_\alpha}{\partial \tilde{r}}, \tag{65}$$

$$\frac{\partial \tilde{p}_\alpha}{\partial \tilde{r}} = \varepsilon^2 \frac{\partial^2 \tilde{v}_\alpha}{\partial \tilde{x}^2} + \frac{\partial^2 \tilde{v}_\alpha}{\partial \tilde{r}^2} + \frac{1}{\tilde{r}} \frac{\partial \tilde{v}_\alpha}{\partial \tilde{r}} - \frac{\tilde{v}_\alpha}{\tilde{r}^2}. \tag{66}$$

• *α-β interface ($\tilde{r} = 1 - \tilde{e}$):*

$$\text{B.C. 8} \quad \frac{\tilde{u}_\alpha}{\mu_\alpha} = \frac{\tilde{u}_\beta}{\mu_\beta}, \quad \text{on } A_{\beta\alpha}, \tag{67}$$

B.C. 9 $$\frac{\tilde{v}_\alpha}{\mu_\alpha} = \frac{\tilde{v}_\beta}{\mu_\beta}, \quad \text{on } A_{\beta\alpha}, \tag{68}$$

B.C. 10 $$\begin{aligned}&\left[\frac{\partial \tilde{u}_\beta}{\partial \tilde{r}} + \varepsilon\frac{\partial \tilde{v}_\beta}{\partial \tilde{x}} - \frac{\partial \tilde{u}_\alpha}{\partial \tilde{r}} - \varepsilon\frac{\partial \tilde{v}_\alpha}{\partial \tilde{x}}\right](1-\varepsilon^2\tilde{e}_{\tilde{x}}^2)+ \\ &+2\left[\varepsilon\frac{\partial \tilde{u}_\beta}{\partial \tilde{x}} - \frac{\partial \tilde{v}_\beta}{\partial \tilde{r}} - \varepsilon\frac{\partial \tilde{u}_\alpha}{\partial \tilde{x}} + \frac{\partial \tilde{v}_\alpha}{\partial \tilde{r}}\right]\varepsilon\tilde{e}_{\tilde{x}} = 0, \quad \text{on } A_{\beta\alpha}\end{aligned} \tag{69}$$

B.C. 11 $$\begin{aligned}&(\tilde{p}_\alpha - \tilde{p}_\beta)(1+\varepsilon^2\tilde{e}_{\tilde{x}}^2) + 2\,\varepsilon^3\tilde{e}_{\tilde{x}}^2\left(\frac{\partial \tilde{u}_\beta}{\partial \tilde{x}} - \frac{\partial \tilde{u}_\alpha}{\partial \tilde{x}}\right) + 2\left(\frac{\partial \tilde{v}_\beta}{\partial \tilde{r}} - \frac{\partial \tilde{v}_\alpha}{\partial \tilde{r}}\right) + \\ &+2\,\varepsilon\tilde{e}_{\tilde{x}}\left[\frac{\partial \tilde{u}_\beta}{\partial \tilde{r}} + \varepsilon\frac{\partial \tilde{v}_\beta}{\partial \tilde{x}} - \frac{\partial \tilde{u}_\alpha}{\partial \tilde{r}} - \varepsilon\frac{\partial \tilde{v}_\alpha}{\partial \tilde{x}}\right] \quad \text{on } A_{\beta\alpha} \\ &= \frac{\varepsilon^2\tilde{e}_{\tilde{x}\tilde{x}}}{(1+\varepsilon^2\tilde{e}_{\tilde{x}}^2)^{1/2}} + \frac{(1+\varepsilon^2\tilde{e}_{\tilde{x}}^2)^{1/2}}{(1-\tilde{e})}.\end{aligned} \tag{70}$$

• *β-phase (free water):*

$$\varepsilon\frac{\partial \tilde{u}_\beta}{\partial \tilde{x}} + \frac{1}{\tilde{r}}\frac{\partial(\tilde{r}\tilde{v}_\beta)}{\partial \tilde{r}} = 0, \tag{71}$$

$$\varepsilon\frac{\partial \tilde{p}_\beta}{\partial \tilde{x}} = \varepsilon^2\frac{\partial^2 \tilde{u}_\beta}{\partial \tilde{x}^2} + \frac{\partial^2 \tilde{u}_\beta}{\partial \tilde{r}^2} + \frac{1}{\tilde{r}}\frac{\partial \tilde{u}_\beta}{\partial \tilde{r}}, \tag{72}$$

$$\frac{\partial \tilde{p}_\beta}{\partial \tilde{r}} = \varepsilon^2\frac{\partial^2 \tilde{v}_\beta}{\partial \tilde{x}^2} + \frac{\partial^2 \tilde{v}_\beta}{\partial \tilde{r}^2} + \frac{1}{\tilde{r}}\frac{\partial \tilde{v}_\beta}{\partial \tilde{r}} - \frac{\tilde{v}_\beta}{\tilde{r}^2}. \tag{73}$$

• *β-σ interface ($\tilde{r} = 1$):*

B.C. 12 $$\tilde{u}_\beta = 0 \quad \text{on } A_{\beta\alpha}, \tag{74}$$

B.C. 13 $$\tilde{v}_\beta = 0 \quad \text{on } A_{\beta\alpha}. \tag{75}$$

Asymptotic development can now be inserted in the above equations by making use of the expansion given in Einstein's notation by (Aziz, 1988)

$$\tilde{a} = \varepsilon^{\mathrm{i}}\tilde{a}_{\mathrm{i}} \tag{76}$$

for $\tilde{a}$ representing velocities and pressures. Doing so leads to a succession of problems at increasing order in ε. The 0th and 1st order problems are respectively given by

• 0*th order:*

$$\frac{\partial(\tilde{r}\tilde{v}_\alpha^0)}{\partial \tilde{r}} = 0, \tag{77}$$

$$\frac{\partial^2 \tilde{u}_\alpha^0}{\partial \tilde{r}^2} + \frac{1}{\tilde{r}} \frac{\partial \tilde{u}_\alpha^0}{\partial \tilde{r}} = 0, \tag{78}$$

$$\frac{\partial \tilde{p}_\alpha^0}{\partial \tilde{r}} = \frac{\partial^2 \tilde{v}_\alpha^0}{\partial \tilde{r}^2} + \frac{1}{\tilde{r}} \frac{\partial \tilde{v}_\alpha^0}{\partial \tilde{r}} - \frac{\tilde{v}_\alpha^0}{\tilde{r}^2}. \tag{79}$$

B.C. 14 $$\frac{\tilde{u}_\alpha^0}{\mu_\alpha} = \frac{\tilde{u}_\beta^0}{\mu_\beta} \quad \tilde{r} = 1 - \tilde{e}, \tag{80}$$

B.C. 15 $$\frac{\tilde{v}_\alpha^0}{\mu_\alpha} = \frac{\tilde{v}_\beta^0}{\mu_\beta} \quad \tilde{r} = 1 - \tilde{e}, \tag{81}$$

B.C. 16 $$\frac{\partial \tilde{u}_\alpha^0}{\partial \tilde{r}} = \frac{\partial \tilde{u}_\beta^0}{\partial \tilde{r}} \quad \tilde{r} = 1 - \tilde{e}, \tag{82}$$

B.C. 17 $$\tilde{p}_\alpha^0 - \tilde{p}_\beta^0 + 2\left(\frac{\partial \tilde{v}_\beta^0}{\partial \tilde{r}} - \frac{\partial \tilde{v}_\alpha^0}{\partial \tilde{r}}\right) = \frac{1}{(1-\tilde{e})}, \quad \tilde{r} = 1 - \tilde{e}, \tag{83}$$

$$\frac{\partial (\tilde{r} \tilde{v}_\beta^0)}{\partial \tilde{r}} = 0, \tag{84}$$

$$\frac{\partial^2 \tilde{u}_\beta^0}{\partial \tilde{r}^2} + \frac{1}{\tilde{r}} \frac{\partial \tilde{u}_\beta^0}{\partial \tilde{r}} = 0, \tag{85}$$

$$\frac{\partial \tilde{p}_\beta^0}{\partial \tilde{r}} = \frac{\partial^2 \tilde{v}_\beta^0}{\partial \tilde{r}^2} + \frac{1}{\tilde{r}} \frac{\partial \tilde{v}_\beta^0}{\partial \tilde{r}} - \frac{\tilde{v}_\beta^0}{\tilde{r}^2}. \tag{86}$$

B.C. 18 $$\tilde{u}_\beta^0 = 0 \quad \tilde{r} = 1 \tag{87}$$

B.C. 19 $$\tilde{v}_\beta^0 = 0, \quad \tilde{r} = 1. \tag{88}$$

• 1*st order:*

$$\frac{\partial \tilde{u}_\alpha^0}{\partial \tilde{x}} + \frac{1}{\tilde{r}} \frac{\partial (\tilde{r} \tilde{v}_\alpha^1)}{\partial \tilde{r}} = 0, \tag{89}$$

$$\frac{\partial \tilde{p}_\alpha^0}{\partial \tilde{x}} = \frac{\partial^2 \tilde{u}_\alpha^1}{\partial \tilde{r}^2} + \frac{1}{\tilde{r}} \frac{\partial \tilde{u}_\alpha^1}{\partial \tilde{r}}, \tag{90}$$

$$\frac{\partial \tilde{p}_\alpha^1}{\partial \tilde{r}} = \frac{\partial^2 \tilde{v}_\alpha^1}{\partial \tilde{r}^2} + \frac{1}{\tilde{r}} \frac{\partial \tilde{v}_\alpha^1}{\partial \tilde{r}} - \frac{\tilde{v}_\alpha^1}{\tilde{r}^2}. \tag{91}$$

B.C. 20 $$\frac{\tilde{u}_\alpha^1}{\mu_\alpha} = \frac{\tilde{u}_\beta^1}{\mu_\beta}, \quad \tilde{r} = 1 - \tilde{e}, \tag{92}$$

B.C. 21 $$\frac{\tilde{v}_\alpha^1}{\mu_\alpha} = \frac{\tilde{v}_\beta^1}{\mu_\beta} \quad \tilde{r} = 1 - \tilde{e}, \tag{93}$$

B.C. 22 $$2\left(\frac{\partial \tilde{v}_\alpha^0}{\partial \tilde{r}} - \frac{\partial \tilde{v}_\beta^0}{\partial \tilde{r}}\right)\tilde{e}_{\tilde{x}} - \\ - \frac{\partial \tilde{u}_\alpha^1}{\partial \tilde{r}} - \frac{\partial \tilde{v}_\alpha^0}{\partial \tilde{x}} + \frac{\partial \tilde{u}_\beta^1}{\partial \tilde{r}} + \frac{\partial \tilde{v}_\beta^0}{\partial \tilde{x}} = 0, \quad \tilde{r} = 1 - \tilde{e}, \tag{94}$$

B.C. 23 $$\tilde{p}_\alpha^1 - \tilde{p}_\beta^1 + 2\left(\frac{\partial \tilde{v}_\beta^1}{\partial \tilde{r}} - \frac{\partial \tilde{v}_\alpha^1}{\partial \tilde{r}}\right) + \\ + 2\tilde{e}_{\tilde{x}}\left(\frac{\partial \tilde{u}_\beta^0}{\partial \tilde{r}} - \frac{\partial \tilde{u}_\alpha^0}{\partial \tilde{r}}\right) = 0, \quad \tilde{r} = 1 - \tilde{e}, \tag{95}$$

$$\frac{\partial \tilde{u}_\beta^0}{\partial \tilde{x}} + \frac{1}{\tilde{r}}\frac{\partial (\tilde{r}\tilde{v}_\beta^1)}{\partial \tilde{r}} = 0, \tag{96}$$

$$\frac{\partial \tilde{p}_\beta^0}{\partial \tilde{x}} = \frac{\partial^2 \tilde{u}_\beta^1}{\partial \tilde{r}^2} + \frac{1}{\tilde{r}}\frac{\partial \tilde{u}_\beta^1}{\partial \tilde{r}}, \tag{97}$$

$$\frac{\partial \tilde{p}_\beta^1}{\partial \tilde{r}} = \frac{\partial^2 \tilde{v}_\beta^1}{\partial \tilde{r}^2} + \frac{1}{\tilde{r}}\frac{\partial \tilde{v}_\beta^1}{\partial \tilde{r}} - \frac{\tilde{v}_\beta^1}{\tilde{r}^2}. \tag{98}$$

B.C. 24 $$\tilde{u}_\beta^1 = 0, \quad \tilde{r} = 1, \tag{99}$$

B.C. 25 $$\tilde{v}_\beta^1 = 0, \quad \tilde{r} = 1. \tag{100}$$

The corresponding solutions are readily obtained by analytical integration and use of boundary conditions – except the normal projection of the normal stress jump condition on the α-β interface – as well as axial symmetry of the flow. One finds

$$\tilde{u}_\alpha = \frac{1}{4}\varepsilon\left(\frac{\mathrm{d}\tilde{p}_\alpha^0}{\mathrm{d}\tilde{x}}\right)\left[\tilde{r}^2 - (1-\tilde{e})^2 + 2\frac{\mu_\alpha}{\mu_\beta}(1-\tilde{e})^2 \ln(1-\tilde{e})\right] + \\ + \frac{1}{4}\frac{\mu_\alpha}{\mu_\beta}\varepsilon\left(\frac{\mathrm{d}\tilde{p}_\beta^0}{\mathrm{d}\tilde{x}}\right) \times \\ \times [(1-\tilde{e})^2 - 1 - 2(1-\tilde{e})^2 \ln(1-\tilde{e})] + \mathrm{o}(\varepsilon^2); \tag{101}$$

$$\tilde{v}_\alpha = \mathrm{o}(\varepsilon^2), \tag{102}$$

$$\tilde{u}_\beta = \frac{1}{4}\varepsilon \left(\frac{\mathrm{d}\tilde{p}_\beta^0}{\mathrm{d}\tilde{x}}\right)[\tilde{r}^2 - 1 - 2(1-\tilde{e})^2 \ln \tilde{r}] + \\ + \frac{1}{2}\varepsilon \left(\frac{\mathrm{d}\tilde{p}_\alpha^0}{\mathrm{d}\tilde{x}}\right)(1-\tilde{e})^2 \ln \tilde{r} + \mathrm{o}(\varepsilon^2), \tag{103}$$

$$\tilde{v}_\beta = o(\varepsilon^2). \tag{104}$$

whereas 0th and 1st order pressure gradients are along $\mathbf{e}_x$ only, just as obtained in the lubrication approach.

Appendix 2. On the Physical Relevance of Considering the Same Microscopic Geometrical Characteristics for a Dry and Partially Saturated Piece of Wood

The aim of this section is to discuss the geometrical hypothesis performed in the present paper concerning the position of pore walls during drying in our ideal medium made of a bundle of capillary tubes. Throughout our study, the classical hypothesis that bound water is adsorbed inside the solid matrix has been accepted. Furthermore, it has been assumed that wall positions (free water/solid matrix interface in the non-hygroscopic region and humid air/solid matrix interface in the hygroscopic region) are not modified by the shrinkage that occurs during drying. Our goal is here to provide some justification of these hypotheses on the basis of experimental observations on oak wood samples reported in the literature.

In a recent work (Couture *et al.*, 2000), it was shown that the total volume of pores – measured by mercury porosimetry – on a dry oak wood sample is approximately equal to the free water volume which is present in the same sample, when it is entirely saturated with water. This free water volume was estimated by weighing the sample at three different stages: dry sample, sample at the saturation point – $W = W_{\mathrm{sp}}$ –, sample saturated with water under vacuum conditions – 0.05bar –. It was shown in this work that mercury porosimetry performed on a dry sample gives a good estimation of the volume available for a free phase all along the drying process.

A careful analysis of shrinkage performed on oak wood during drying (Nadeau and Puiggali, 1995; Skarr, 1988) showed that volume reduction only takes place in the hygroscopic region ($W \leqslant W_{\mathrm{sp}}$). Moreover, it was shown that the volume reduction is approximately equal, at each step of the drying, to the volume loss of bound water. As a consequence, and for oak wood at least, the volume of bound water contained in a sample for which initial moisture content is above the saturation point, W_{sp}, can be well estimated from the total shrinkage of the sample measured at the end of a drying process.

In a hygroscopic capillary porous medium, the total titrable water is under three different forms: free water, bound water and vapor. If one assumes that the above mentioned results are transposable at the pore scale, the titrable water distribution

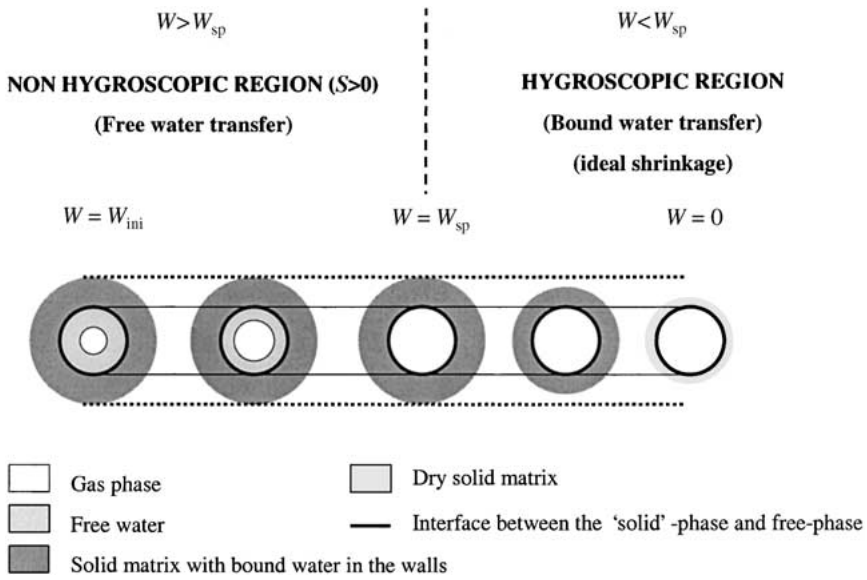

Figure 8. Repartition of the total titrable water in a pore radius.

in a unique pore can be represented as in Figure 8. In the non-hygroscopic region, free water drains and is replaced by gas phase. During this stage, a no-slip condition can be considered between free water and 'solid phase' made of bound water and solid matrix. In the hygroscopic region, bound water is removed and an ideal shrinkage of the 'solid' phase can be considered. All along the drying, the interface between the free phase (free water or gas) and the 'solid' phase is fixed. As a result, if one accepts the transposition of macroscopic observations to the pore-scale, structural data like pore size distribution, intrinsic permeability, capillary pressure curve obtained, for instance, by mercury intrusion on a totally dry medium can be used all along a drying process simulation. As a matter of fact, the pore volume accessible in a dry sample is the pore volumes available for free phase transfer.

References

Auriault, J. L.: 1987, Nonsaturated deformable porous media: quasistatics, *Transport in Porous Media* **2**, 45–64.

Ayub, M. and Bentsen, R. G.: 1999, Interfacial viscous coupling: a myth or reality? *J. Petro. Sci. Engg* **23**, 13–26.

Aziz, A.: 1988, Perturbation methods, in: W. J. Minkowycz, E. M. Sparrow, G. E. Schneider and R. H. Pletcher (eds), *Handbook of Numerical Heat Transfer*, Wiley.

Bacri, J. C., Chaouche, M. and Salin, D.: 1990, Modèles simples de perméabilités relatives croisées, *C.R. Acad. Sci. Paris* **311**, Séries II, 591–597.

Baixeras, O.: 1995, Modélisation et mise en oeuvre expérimentale du séchage sous-vide discontinu du chêne, Thesis, University of Bordeaux 1, France.

Bonneau, P.: 1991, Modélisation du séchage d'un matériau hétérogène: application à un bois de résineux, Thesis, University of Bordeaux 1, France.

Bretherton, F. P.: 1961, The motion of long bubbles in tubes, *J. Fluid Mech.* **10**, 166–188.

Bradley, R. S.: 1936, Polymolecular adsorbed films, Part 2: the general theory of the condensation of vapours on finely divided solids, *J. Chem. Soc.*, 1799–1804.

Ceaglske, N. H. and Hougen, O. A.: 1937, Drying granular solids, *Ind. Eng. Chem.* **29**, 805–817.

Collignan, A.: 1988, Elaboration et utilisation d'une cinétique de séchage – Application à un bois de résineux, Thesis, University of Bordeaux 1, France.

Comstock, G. L.: 1970, Directional permeability of softwoods. *Wood Fiber* **1**, 283–289.

Couture, F.: 1995, Modélisation fine d'un problème de séchage. Développement d'outils adaptés, Thesis, University of Bordeaux 1, France.

Couture, F., Jomaa, W. and Puiggali, J. R.: 1996, Relative permeability relations: a key factor for a drying model, *Transport in Porous Media* **23**, 303–335.

Couture, F., Jomaa, W. and Puiggali, J. R.: 2000, Prise en compte du volume d'eau liée dans la modélisation du séchage d'un milieu capillaro-poreux hygroscopique, Internal Report. LEPT-ENSAM.

Derjaguin, B.: 1943, Thickness of liquid layer adhering to walls of vessels on their emptying and the theory of photo- and motion picture film coating, *Comptes Rendus (Doklady) de l'Académie des Sciences de l'URSS* **39**(1), 13–16.

Dullien, F. A. L.: 1979, *Porous Media – Fluid Transport and Pore Structure*, New York, Academic Press.

Dullien, F. A. L., Zarcone, C., McDonald I. F., Collins, A. and Bochard, R. D. E.: 1989, The effect of surface roughness on the capillary pressure curves and the heights of capillary rise in glass bead packs, *J. Colloid Interface Sci.* **127**(2), 362–372.

Ehrlich, R., Etris, E. L., Brumfield, D., Yuan, L. P. and Crabtree, S. J.: 1991, Petrography and reservoir physics III: physical models for permeability and formation factor, *The American Association of Petroleum Geologists Bulletin* **75**(10), 1579–1592.

Ferguson, W. J. and Turner, I. W.: 1994, Unstructured numerical solutions techniques applied to timber drying problems, in: *Proceeding of the 9th International drying Symposium, B*, 719–726.

Guilmain, C.: 1997, Analyse et modélisation d'un procédé de séchage sous vide en vapeur d'eau surchauffée – Application au bois de chêne, Thesis, ENSAM, France.

Hernandez, J. M.: 1991, Séchage du chêne, caractérisation, procédés convectif et sous vide, Thesis, University of Bordeaux 1, France.

Israelachvili, J. N.: 1985, *Intermolecular and Surface Forces*, Academic Press, London.

Kaviany, M. and Mittal, M.: 1987, Funicular state in drying of a porous slab, *Int. J. Heat and Mass Transfer* **30**(7), 1407–1418.

Landau, L. and Levich, B.: 1942, Dragging of a liquid by a moving plate, *Acta Physicochimica, USSR* **17**(1.2), 42–54.

Lasseux, D. and Quintard, M.: 1991, Epaisseur d'un film dynamique derrière un ménisque récessif, *C. R. Acad. Sci. Paris* **313**(II), 1375–1381.

Lasseux, D., Quintard, M. and Whitaker, S.: 1996, Determination of permeability tensors for two-phase flow in homogeneous porous media: theory, *Transport in Porous Media* **24**, 107–137.

Laurindo, J. B.: 1996, Evaporation en milieu poreux. Etude expérimentale sur milieux modèles et modélisation de type percolation, Thesis, INP, Toulouse, France.

Laurindo, J. B. and Prat, M.: 1998a, Modeling of drying in capillary porous media: a discrete approach, *Drying Technology* **16**(9&10), 1769–1787.

Laurindo, J. B. and Prat, M.: 1998b, Numerical and experimental network study of evaporation in capillary porous media. Drying rates, *Chem. Engg Sci.* **53**(12), 2257–2269.

Lewis, W. K.: 1921, The rate of drying of solids materials, *Ind. Eng. Chem.* **13**(5), 427–432.

Mason, E. A. and Malinauskas, A. P.: 1983, *Gas Transport in Porous Media: The Dusty Gas Model, Chemical Engineering Monographs*, Elsevier.

Moyne, C.: 1987, Transferts couplés chaleur-masse lors du séchage: prise en compte du mouvement de la phase gazeuse, Thesis, University of Nancy, France.

Nadeau, J. P. and Puiggali, J. R.: 1995, *Le Séchage: Des Processus aux Procédés Industriels*, TEC & DOC Lavoisier, Paris.

Perré, P. and Degiovanny, A.: 1990, Simulations par volumes finis des transferts couplés en milieux poreux anisotropes: séchage du bois à basse et haute température, *Int. J. Heat and Mass Transfer* **33**(11), 2463–2478.

Perré, P. and Moyne, C.: 1991, Processes related to drying: part II, use of the same model to solve transfers both in saturated and unsaturated porous media, *Drying Technology* **9**(5), 1153–1179.

Perré, P. and Turner, I.W.: 1999, Transpore: a generic heat and mass transfer computational model for understanding and visualising the drying of porous media, *Drying Technology* **17**(7 & 8), 1273–1289.

Plumb, O. A., Spolek, G. A. and Olmstead, B. A.: 1985, Heat and mass transfer in wood during drying, *Int. J. Heat and Mass Transfer* **28**(9), 1669–1678.

Puiggali, J. R. and Quintard, M.: 1992, Properties and simplifying assumptions for classical drying models, *Advances in drying* **5**, 131–147.

Quéré, D.: 1999, Fluid coating on a fiber, *Annu. Rev. Fluid Mech.* **31**, 347–384.

Siau, J. F.: 1984, *Transport Processes in Wood*, Springer-Verlag.

Skaar, C.: 1985, *Wood-Water Relations*, Springer-Verlag.

Spolek, G. A. and Plumb, O. A.: 1981, Capillary pressure in softwoods, *Wood Sci. Technol*. **15**, 189–199.

Whitaker, S.: 1977, Simultaneous heat, mass and momentum transfer in porous media: a theory of drying, *Advances in Heat Transfer* **13**, 119–203.

Whitaker, S.: 1984, Moisture transport mechanisms during the drying of granular porous media, in: *Proceeding of the 4th International Drying Symposium* 1, 31–42.

Whitaker, S.: 1986, Flow in porous media II: the governing equations for immiscible two-phase flow, *Transport in Porous Media* 1, 105–125.

Whitaker, S. and Chou, W. T. H.: 1983–84, Drying of granular porous media – theory and experiment, *Drying Technology* **1**(1), 3–33.